

Review

The Use of Copper-Based Delafossite to Improve Hydrogen Production Performance: A Review

Hasnae Chfii *, Amal Bouich * and Bernabé Mari Soucase

Departament de Física Aplicada, Institut de Disseny i Fabricació (IDF), Universitat Politècnica de València, 46022 Valencia, Spain; mari@fis.upv.es

* Correspondence: hasnaechfii@gmail.com (H.C.); bouich.amal@gmail.com (A.B.)

Abstract: This review paper reports on the use of Delafossite as a layer between perovskite-based solar cells to improve hydrogen production efficiency and make the process easier. The investigation delves into the possible breakthroughs in sustainable energy generation by investigating the synergistic interplay between Delafossite and solar technology. This investigation covers copper-based Delafossite material's properties, influence on cell performance, and function in the electrolysis process for hydrogen production. Some reports investigate the synthesis and characterizations of delafossite materials and try to improve their performance using photo electrochemistry. This work sheds light on the exciting prospects of Delafossite integration using experimental and analytical methodologies.

Keywords: delafossite; photovoltaic cells; hydrogen; thin films; performance

1. Introduction

Hydrogen (H₂) stands out as a crucial, eco-friendly, abundant, and safe alternative in the realm of renewable energy, poised to address the escalating need for sustainable and clean power. Widely regarded as one of the most environmentally friendly energy sources, hydrogen holds significant promise in mitigating both the energy crisis and climate change [1–9]. Furthermore, its application in electricity generation in various industrial settings brings the added benefit of minimal nitrous and sulfur oxide emissions. Notwithstanding these advantages, challenges persist in the efficient processing and storage of hydrogen, hindering the full realization of a hydrogen-based energy economy. Notably, security issues about hydrogen storage, transportation, and transportation remain common [10–17]. Current conventional hydrogen storage methods, employing various metal hydrides, fall short in terms of storage capacity. Hence, there is a pressing need to develop a hydrogen storage system based on fuel cells to address this limitation [18–24]. H₂ fuel cell systems, characterized by their low carbon emissions and high efficiency, are emerging as compelling alternatives to internal combustion engines in the automotive sector [25–31]. The environmental benefits, increased efficiency, and burgeoning global interest in hydrogen fuel cell systems underscore their growing prominence in recent years. Photocatalysts, relying on either photo-electrocatalysis or direct photocatalysis, engage in processes that hinge on incoming light-induced electron production and transport between electrodes (Figure 1).

When electrodes are made of a photoactive material, including a semiconductor (SC), this method can be implemented. The photoanode in this configuration is made of an n-type SC, whereas the photocathode is made of a p-type SC. Figure 1 depicts the operating principle of the resultant photoelectrochemical cell (PEC). The core idea of a photocatalysis system is the promotion of water breakdown utilizing solar energy, propelling the photoactive material to generate photoexcited charge carriers, ultimately yielding hydrogen. The process unfolds in the following steps: [5] (i) The photoanode absorbs solar light, producing holes and electrons. (ii) Holes as well as electrons travel



Citation: Chfii, H.; Bouich, A.; Soucase, B.M. The Use of Copper-Based Delafossite to Improve Hydrogen Production Performance: A Review. *Hydrogen* **2024**, *5*, 39–58. <https://doi.org/10.3390/hydrogen5010004>

Academic Editor: Zhang-Hui Lu

Received: 25 December 2023

Revised: 24 January 2024

Accepted: 24 January 2024

Published: 30 January 2024



Copyright: © 2024 by the authors. Licensee MDPI, Basel, Switzerland. This article is an open access article distributed under the terms and conditions of the Creative Commons Attribution (CC BY) license (<https://creativecommons.org/licenses/by/4.0/>).

from one electrode to the next. (iii) Chemical processes make it easier to remove H_2 and O_2 from water molecules [31–35].

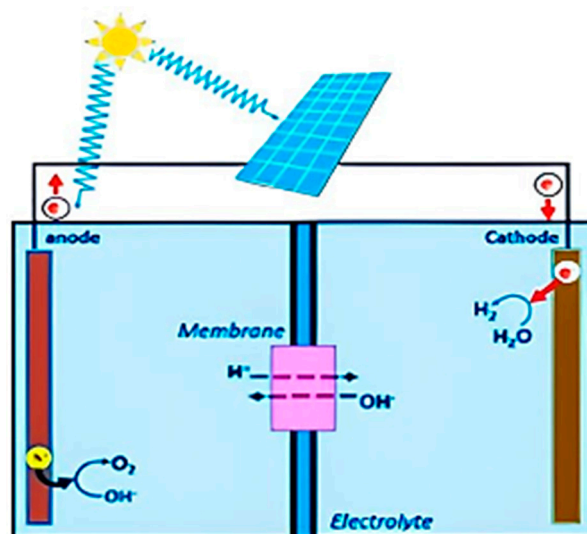


Figure 1. Photoelectrochemical (PEC) system scheme: integration of photoelectrode into PV-cell-powered configuration [32].

In accordance with the analysis conducted by the International Energy Agency (IEA) on the global total final energy consumption, the share of hydrogen energy in overall energy consumption is anticipated to rise to approximately 2% by 2030 and around 10% by 2050. This escalation is imperative for achieving the net-zero plan concurrently with a substantial reduction in the consumption of nonrenewable fossil fuels. Furthermore, the levels of total final energy consumption derived from renewables are expected to witness an increase of about 0.51% by 2030 and approximately 7.41% by 2050 compared to the levels in 2020. The growing demand for renewables will propel electricity consumption, surging from roughly 19.13% in 2020 to around 26.28% in 2030 and a notable 49.23% in 2050. It is noteworthy that intermittent renewables can be converted into electricity through power stations integrated into grids, with surplus electricity being employed in the production of hydrogen through electrolysis. The effective interconversion of hydrogen and electricity is facilitated by fuel cells and electrolyzers. In light of these dynamics, it is evident that hydrogen is poised to assume a pivotal and irreplaceable role in shaping the future landscape of long-term energy systems [36].

In the quest for an ideal semiconductor (SC) material, certain criteria must be met to ensure optimal performance. Specifically, the material's band gap (E_g) must surpass $\{E^\circ(O_2/H_2O) - E^\circ(H_2O/H_2)\}$, with the conduction band (ECB) situated below $E^\circ(H_2O/H_2)$ and the valence band (EVB) positioned above $E^\circ(O_2/H_2O)$. Accounting for overpotentials that frequently reach 1 V, a material's E_g must exceed 2.2 eV for effective water cleavage. Notably, many stable oxides are exclusively absorbed in the UV region, making them impracticable for efficient solar spectrum use since their E_g values are too high. To overcome this problem, research attention has recently shifted to narrow-band-gap SCs, particularly in the context of H_2 generation. The exploration of novel materials using electronic bands formed from cationic orbitals is an interesting method. The oxides, which have the general formula $Cu^+M^{3+}O_2$ and crystallize in the delafossite structure, have VB and CB bands that originate from Cu 3d orbitals with d-d photo transitions. M represents rare earth or a three-dimensional metal in this context. These materials are pH-insensitive and may be precisely matched with electrolyte levels at a specific pH [37–41].

Delafossite compounds, notably $CuMO_2$ (Figure 2), in which the M sites are filled by boron group elements, transition metals, or rare-earth elements, have attracted a lot of attention over the past few decades. This renewed attention stems from their prospective uses, which range from serving as electrodes for hydrogen generation via photoelectrochemical

(PEC) water splitting to functioning as transparent conductive oxides in optoelectronic devices. Additionally, these compounds are being explored for their potential roles in spintronic and ferroelectric devices [42–48].

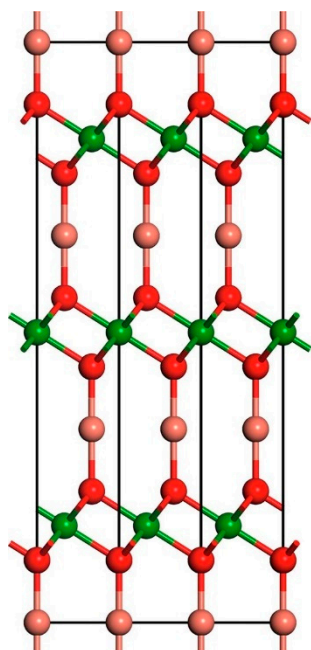


Figure 2. Crystal model of CuMO₂ delafossite, where (●) is Cu, (●) is M, and (●) is O.

2. Delafossite Used in Water-Splitting Systems for Hydrogen Production

In the presence of water, separated electrons participate in the reduction reaction, converting water molecules (H₂O) into hydrogen gas (H₂). Simultaneously, the holes contribute to the oxidation reaction, producing oxygen gas (O₂) [49–54].

- Reduction Reaction:

$$2\text{H}_2\text{O} + 2\text{e}^- \rightarrow \text{H}_2 + 2\text{OH}^-$$
- Oxidation Reaction:

$$4\text{H}_2\text{O} \rightarrow 4\text{e}^- + \text{O}_2 + 4\text{H}^+$$
- Photoelectrochemical (PEC) System:

Photo electrochemistry is dependent on the excited state of a semiconductor achieved using suitable light quantities ($h\nu > E_g$). This excitation automatically generates an electric junction force between the two phases, allowing electron–hole pairs produced by photons to be separated. Photoelectrons in the conduction band generate cathodic hydrogen on the surface catalyst, but photo holes in the valence band move in opposite directions to aid in the anodic decomposition process [55–59]. This simultaneous oxidation and reduction process takes place on opposite poles within the crystallite, mimicking a photoelectrochemical diode and eliminating the need for elaborate and costly electrochemical equipment. The electrolytic solution closes the circuit with little electrical resistance [60–64]. Because of its fascinating features, including its ability to modulate optical gaps and lattice constants, the CuMO₂ family has sparked interest in light–energy conversion. A notable example is CuYO₂, representing a host lattice with the ability to intercalate anionic species, a focal point in hydrogen energy research [65–69].

A cost-effective approach to harnessing solar energy for fuel generation via water splitting involves utilizing a D4-type photoelectrochemical (PEC) tandem cell. This configuration consists of a connected n-type semiconductor photoanode and a p-type semiconductor photocathode. Despite the success in developing robust and cost-effective photoanode materials (e.g., WO₃, Fe₂O₃, and BiVO₄) with respectable photocurrents and high stability,

the search for reliable and affordable p-type photocathodes continues [70–75]. Several p-type semiconductors, including p-Si, p-GaInP₂, and p-WSe₂, have exhibited exceptional performance. However, their widespread production faces challenges due to expensive and energy-intensive deposition or processing procedures. Notably, copper-based materials like p-Cu₂O, p-CuGaSe₂ (CGS), and p-Cu₂ZnSnS₄ (CZTS) have recently emerged as promising alternatives for p-type photocathodes, garnering attention for their potential in this role. These materials, which are based on plentiful amounts of copper, work well, even with solution-based deposition processes, allowing for large-scale deposition. However, difficulties continue since chalcogenides sometimes require a hazardous cadmium sulfide overlayer, and stability concerns, notably regarding copper(I) oxide, have developed [76–78].

An effective technique for addressing these difficulties includes covering the absorbent material with a conformal protective layer. Ensuring the hermeticity of this layer is crucial to prevent the degradation of the absorbing layer and maintain a thin profile to mitigate resistance losses. However, this approach introduces complexity to the manufacturing process and elevates the cost of the photoelectrodes [79–84]. To facilitate the development of cost-effective and easily scalable photoelectrochemical (PEC) devices, it is imperative to identify an intrinsically stable p-type material for water photoreduction. In this context, copper-based delafossite materials like CuCrO₂ [85–88], CuAlO₂ [86,87,89], CuGaO₂ [87,88], and CuFeO₂ [87,88] have demonstrated notable water stability. Furthermore, CuFeO₂ [90,91] and CuRhO₂ have recently been postulated to be possible water reduction photocathodes.

The reductive HER mechanism in copper-based delafossite materials involves intricate processes occurring at the semiconductor–electrolyte interface, with potential structural reconstructions influencing the overall efficiency of the reaction. As photons with energy greater than the bandgap ($h\nu > E_g$) are absorbed by the semiconductor, electron–hole pairs are generated, initiating the HER process. In the specific case of CuMO₂ (where M represents various metal elements), the conduction band electrons are harnessed for the reduction of protons to form hydrogen gas, while the photo-generated holes may be involved in concurrent anodic processes.

Before HER initiation, the delafossite structure, characterized by layered arrangements of metal cations, may undergo transformations in response to interaction with the electrolyte. This interaction can lead to changes in the oxidation states of copper ions and alterations in the coordination environment, potentially facilitating the subsequent HER steps.

During and after an HER, the semiconductor–electrolyte interface plays a crucial role in governing the reaction kinetics. The intricate interplay involves the adsorption of protons, charge transfer processes, and the release of hydrogen gas. Any structural reconstruction during the HER may impact the catalytic sites, influencing the overall efficiency and stability of the photocatalyst.

This mechanistic insight provides a foundation for understanding the complexities of reductive HERs in copper-based delafossite materials. It is essential to consider these processes to optimize the performance of these materials in sustainable energy applications.

3. CuFeO₂ Delafossite Materials

As emphasized by Mathieu S et al., the literature underscores CuFeO₂'s nature as a promising candidate for solar water reduction. However, it is crucial to continue to attempt to optimize doping and enhance charge separation efficiency in sacrificial electrolytes. Additionally, the semiconductor interface requires optimization using suitable overlayers or catalysts to reduce the reported overpotential necessary for water reduction. The study by Mathieu S et al. showcased a sol–gel-based method for producing thin films of p-type delafossite CuFeO₂ on FTO glass. Our citrate–nitrate technique outperforms previously described methods for preparing CuFeO₂ for photoelectrochemical (PEC) research [92]. These advantages encompass straightforward solution processing of the films, a comparatively low heating temperature required for delafossite phase generation, and the ability to

tailor layer thickness. Rigorous physical characterization confirmed the films' purity and crystal phase. Notably, CuFeO_2 films exhibited an excellent band-edge location, featuring an optical bandgap energy conducive to high-efficiency water splitting in an integrated tandem system. As shown in Figure 3, in the presence of sacrificial electron acceptors, the J–V curves of unaltered CuFeO_2 electrodes demonstrated record photocurrent densities for bare films, with a noteworthy photocurrent initiation at +0.9 V versus a reversible hydrogen electrode (RHE). Furthermore, the incident photon-to-current efficiency onset was determined to be 830 nm. The bare electrodes displayed impressive durability under operating settings for several days, distinguishing CuFeO_2 from other photocathodes. Typically, protective coatings are essential to ensure the survival of materials under corrosive conditions, particularly in reductive environments [93,94].

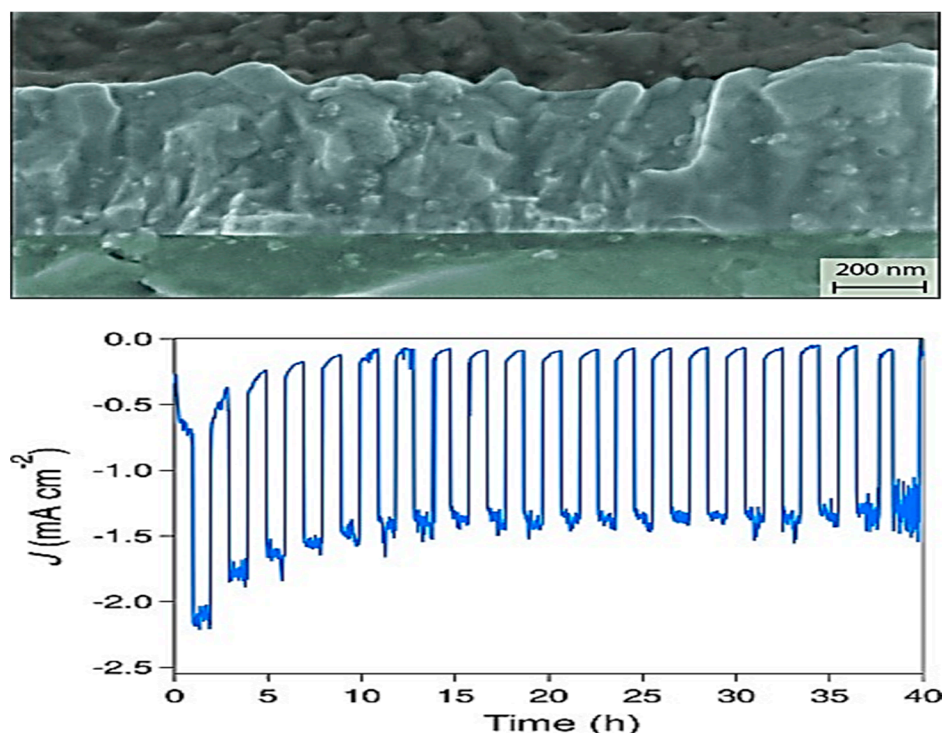


Figure 3. A view of many layers of CuFeO_2 film on FTO, and chronoamperometry of a CuFeO_2 electrode under O_2 -bubbling and chopped illumination conditions [70].

Another pertinent study conducted by Carrier et al. showcased a straightforward electrochemical synthesis method for thin CuFeO_2 electrodes. Their research demonstrated the thermodynamic possibility of generating H_2 photoelectrochemically while absorbing the whole visible spectrum [95]. Future efforts will concentrate on adjusting deposition conditions; we are exploring alternative techniques for creating CuFeO_2 electrodes with optimal thicknesses and morphologies. Additionally, our research involves identifying suitable H_2 evolution catalysts for integration onto the surface of CuFeO_2 (Figure 4). This strategy attempts to improve the effectiveness of CuFeO_2 photocathodes for splitting water using photoelectrochemical techniques [96].

Furthermore, we are conducting investigations into the utilization of p- CuFeO_2 as a photocathode for the reduction of CO_2 , exploring the potential advantage of its less-favorable catalytic characteristics for H_2 evolution. The current work investigated the photoelectrochemical generation of H_2 without stirring utilizing electrode-type CuFeO_2 , ruling out the potential of mechano-catalytically creating H_2 . Nevertheless, due to the limited steady-state photocurrent attained for water reduction, generating a measurable quantity of H_2 from a thin CuFeO_2 film using the current setup proved challenging [97]. Attempts to boost H_2 production by increasing illumination intensity failed because increased

intensity resulted in large concentrations of photogenerated electrons on the outside of the CuFeO_2 , leading to photo corrosion. Surprisingly, the inclusion of O_2 in the electrolyte reduced severe photo corrosion when more powerful light was used. An idea was developed wherein creating a photocurrent in an environment of O_2 , which improves CuFeO_2 photo-stability under high light, would increase the possibility of detecting H_2 . Even with a poor photocurrent-to- H_2 conversion efficiency, any amount of H_2 discovered in this experiment would indicate the thermodynamic feasibility of solar H_2 synthesis by CuFeO_2 [98].

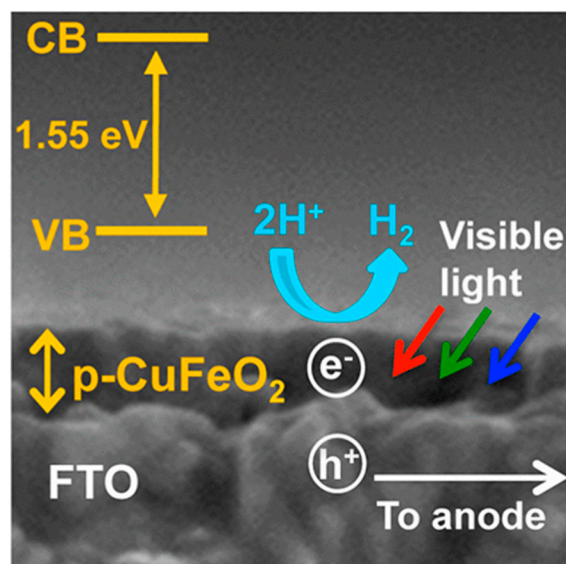


Figure 4. A schematic and a cross section of p-CuFeO_2 thin film on FTO [95].

4. CuCrO_2 Delafossite Materials

In a notable study, S. Saad et al. investigated the technical feasibility of photochemical hydrogen (H_2) evolution by employing a mix of CuCrO_2 powder in electrolytes composed of water with various reducing agents (SO_3^{2-} , (insert another reducing agent), and $\text{S}_2\text{O}_3^{2-}$). Electrochemical assessments were conducted at 23°C using a Pyrex cell fitted with a Pt counter electrode and an electrode made of saturated calomel (SCE). A deoxygenated promoting electrolyte (1 M KOH) was used, and potentials were recorded using a Voltalab 201 potentiostat. The photoactivity experiments were conducted in a 600 mL double-jacketed cell at $50 \pm 0.1^\circ\text{C}$, which was illuminated by three 200 W tungsten lamps. Gas chromatography was used to identify hydrogen, and a coaxial switched burette was used to estimate its volume. A Jenway 6051 spectrometer was used to calorimetrically quantify the concentration of yellow polysulfide Sn^{2-} at $\text{max} = 520\text{ nm}$. Once-distilled water and A.R.-grade reagents were used to make solutions that could be neutralized with Na_2HPO_4 and NaH_2PO_4 (Figure 5) [99].

The chosen oxide exhibits significant corrosion resistance and possesses an optimal band gap (E_g) of 1.32 eV. The deliberate introduction of a small quantity of oxygen was anticipated to induce the partial oxidation of Cu^+ to Cu^{2+} , resulting in the material acquiring p-type semiconductivity. The oxidation of S_2 is critical for photocorrosion inhibition, and H_2 evolution rises concurrently with the synthesis of Sn^{2-} polysulfides. Notably, when p-CuCrO_2 is coupled with in situ created $\text{n-Cu}_2\text{O}$, a large amount of H_2 is produced. H_2 is primarily liberated on CuCrO_2 , whereas S_2 is oxidized on the Cu_2O surface. The $\text{Cu}_2\text{O/CuCrO}_2$ hetero system has been improved in terms of several physical properties [100].

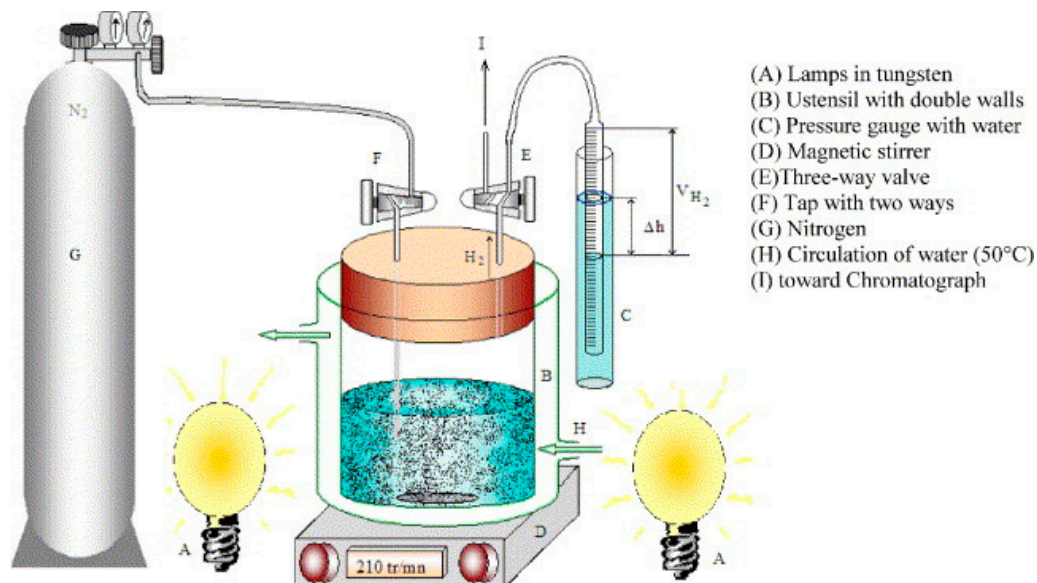


Figure 5. A device for measuring the volume of hydrogen in experimental settings [99].

The photoactivity was found to be conditional and reducing the synthesis temperature using the nitrate approach enhanced specific surface area (S_{sp}). Due to electrons' poor mobility, the arrival of electrons at the contact was designated as the rate-determining phase in the framework of photoelectrochemical H_2 generation [101].

$CuCrO_2$, a p-type semiconductor with a delafossite structure, has received a lot of interest in relation to photocatalysis and solar cells because of its effective absorption of visible light. While cuprous oxide (Cu_2O) shows potential as a photocathode, its chemical stability is limited due to its sensitivity to corrosion when exposed to light. $CuCrO_2$, on the other hand, stands out as an attractive option for photocatalytic applications due to its outstanding chemical stability, p-type semiconductor characteristics, and ability to absorb visible light. Previous research has demonstrated its capacity to create hydrogen from water and remove metal ions when exposed to visible light [102]. Notably, Mg-doped $CuCrO_2$ has demonstrated improved photocatalytic hydrogen generation activity. However, issues such as reduced hydrogen synthesis after short light exposure necessitate additional investigation.

Yi Ma et al. have investigated the photocatalytic H_2 generation capability of $CuCrO_2$ in conjunction with co-catalysts, using water and ethanol as sacrificial reagents. Their study revealed that $CuCrO_2$ has a consistent H_2 generation rate over a 3 h timeframe (Figure 6). Their study proceeded to investigate the photoelectrochemical (PEC) properties of $CuCrO_2$, confirming its p-type semiconductor features. A cathodic photocurrent, a common property of light excitation, was detected and grew stronger as the calcination temperature rose [103–106]. According to the findings, greater calcination temperatures minimize flaws by functioning as recombination centers. $CuCrO_2$'s steady hydrogen generation activity makes it a suitable material for solar-to-energy applications. However, co-catalysts, notably Pt, are thought to be required for effective hydrogen creation during water splitting. Combinations with other semiconductor materials may increase the stability and efficiency of $CuCrO_2$, potentially leading to the creation of efficient p–n junction materials [107].

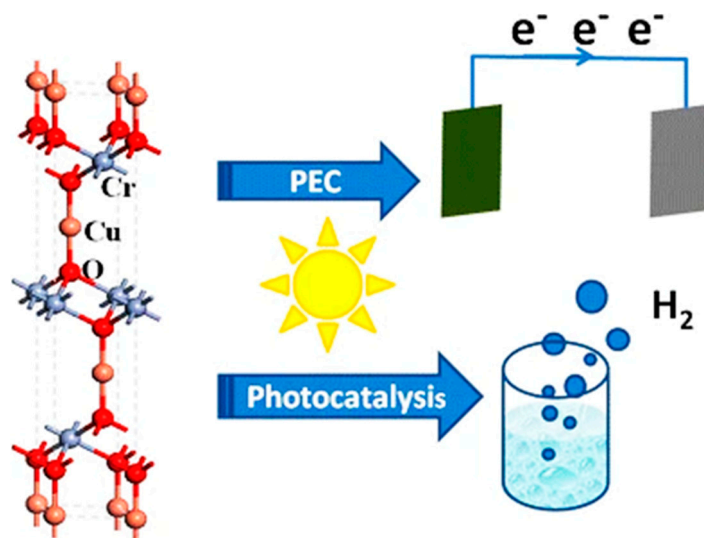


Figure 6. Photocatalytic and photoelectrochemical (PEC) devices for water splitting [106].

5. CuAlO₂ Delafossite Materials

A study focusing on hydrogen production utilizing CuAlO₂ delafossite was conducted by N. Koriche and colleagues. They reported H₂ generation via the simultaneous oxidation of inorganic compounds in a CuAlO₂ solution, constituting a process that is particularly effective when targeting certain processes since S²⁻ oxidizes faster than H₂O. Nevertheless, the photovoltage created was inadequate for electrolysis, necessitating an extra voltage of about 0.5–0.75 V since the VB is significantly lower than the O₂/H₂O potential. Semiconductors typically exhibit a higher O₂ overpotential, often close to 1 V [108].

CuAlO₂ is a semiconductor of the p type with limited-mobility polarons due to its tiny band gap. Its catalytic aptitude for visible-light-induced H₂ generation was studied in connection to the synthesis technique. The conduction band's potential (−1.63 V versus SCE) is lower than the H₂O/H₂ level, allowing for spontaneous H₂ evolution. Coprecipitation resulted in increases in oxide activity. Maximum H₂ generation was reported in a 0.1 M S²⁻ mixture at pH 13.72, with an output rate equal to 0.19 mL h⁻¹ mg⁻¹. As seen in Figure 7, this production increased in tandem with the formation of polysulfide Sn²⁻ (nS²⁻ + 2(n - 1) H₂O Sn²⁻ + (n - 1) H₂ + 2(n - 1)OH⁻). Both processes proceeded concurrently, with no observable photoactivity under pH 7, showing that S²⁻ played a critical role. Carriers were transferred iso-energetically between CuAlO₂ and the electrolyte, with the help of produced band gap states acting as strong relays [109]. The overall reaction is governed by the momentary arrival rate of electrons at the contact, and the greater thermal photoactivity observed is connected to enhanced electronic mobility [110].

In another study, Smith and colleagues explored a thermal-photocatalytic process using dispersed CuAlO₂ catalyst nanoparticles in water under conditions of sunlight exposure. In the experimental setup, depicted in Figure 8, sunlight was used as the primary source of solar radiation, aligning the hydrogen generation container axis with the sun [111]. Solar heating was complemented with electrical resistance heating to elevate the water temperature, and no electrodes were placed in the water to prevent ion currents that may cause photocorrosion. The technique was stable and did not produce any ion currents. The cylinder was linked to a gas chromatograph to test the H₂ concentration throughout typical runs lasting one to multiple hours.

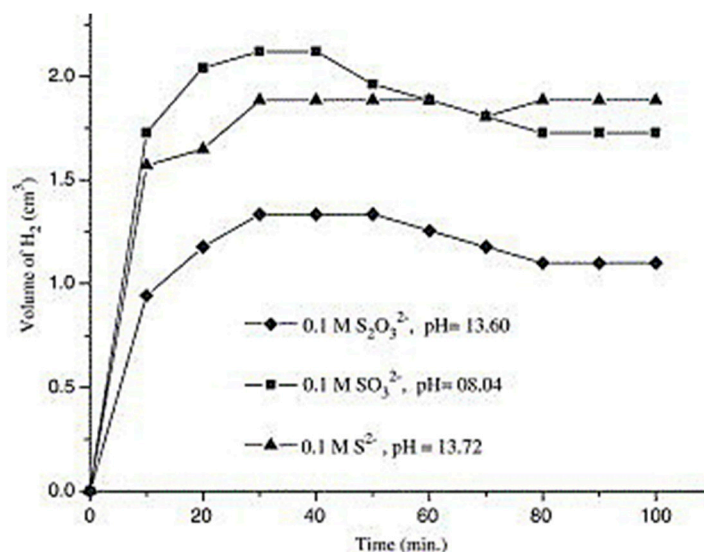


Figure 7. The volume of H₂ evolved as a function of illumination time was investigated for different redox couples in buffered electrolytes [109].

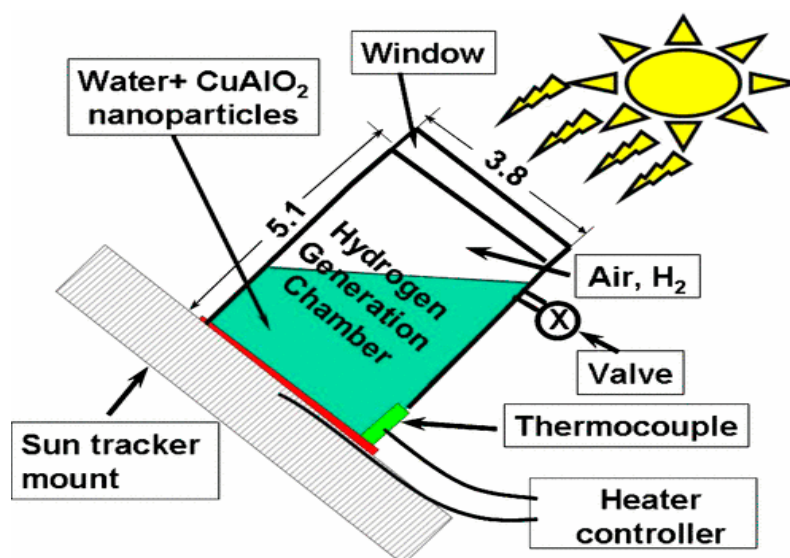


Figure 8. The hydrogen generation apparatus (dimensions are in millimeters) [111].

Due to the known influence of CuAlO₂ band gaps on material preparation parameters, optical absorption tests conducted on thin layers of CuAlO₂ catalyst powders utilized in H₂ production experiments were undertaken [112]. Through absorption coefficient measurement, the films formed over a quartz plate formed using a catalyst that was an aqueous mixture produced both indirect and direct band gap values (Figure 9). The direct gap for the CuAlO₂ particles used was determined to be 3.01 eV, while the indirect gap was 1.87 eV, making both gaps accessible to solar light. Even though indirect-gap transitions require phonon aid in bulk materials, they may be more frequent in tiny catalyst nanoparticles or at higher temperatures.

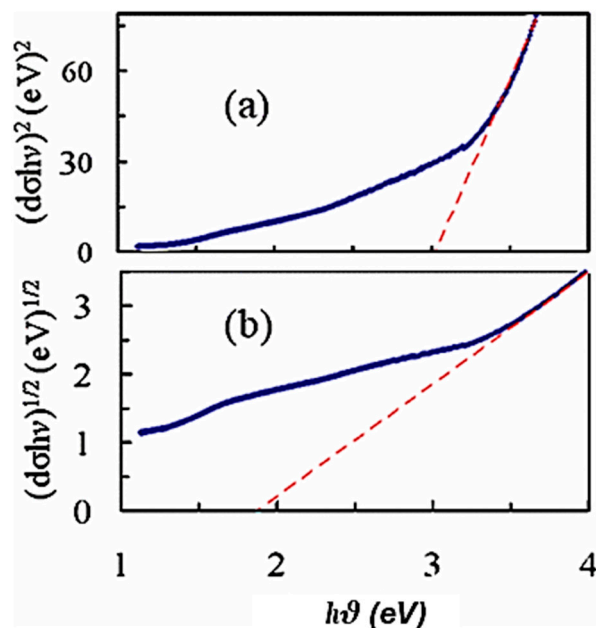


Figure 9. Investigation and determination of the band gaps for our CuAlO₂ powder thin films [112].

A previous study demonstrated photocatalytic H₂ creation for CuAlO₂ in sulfide-doped water at 321 K, with dismal findings of H₂ generation decreasing to zero after a 20–30 min runtime. Notably, corrosiveness was not seen in the experimental environment of CuAlO₂ in H₂O. The measured thermal activation barrier was 0.94 eV. First-principles calculations showed that H₂ desorption is the most actively demanding stage in the H₂ production process. The proposed technique for producing H₂ uses thermal desorption, which is facilitated by a drop in the adsorption barriers produced by solar radiation, allowing contributions to H₂ production from the visible, ultraviolet, and infrared radiation portions of the solar spectrum [113].

6. CuRhO₂ Delafossite Materials

The study of polycrystalline CuRhO₂, acting like a photocathode for visible-light water splitting, reveals its distinct band edge locations that cover the redox potentials associated with water oxidation and reduction. Photogenerated band conduction electrons can decrease water energetically, whereas related valence band holes may oxygenate water and thus make O₂. In an air-saturated solution, visible light triggers H₂ generation with a 0.2 V underpotential [114]. H₂ generation in an Ar-saturated solution, on the other hand, is unstable due to the decrease in the semiconductor producing Cu(s). Notably, in spite of the presence of oxygen, no bulk Cu(s) is discovered, implying that CuRhO₂ may self-heal in the presence of air, resulting in steady H₂ production with roughly 80% Faradaic efficiency.

Jin Gu researched the photoelectrochemistry and manufacture of a p-type CuRhO₂ electrode [115]. The researchers investigated the photostability and water reduction behavior of oxygen- and argon-saturated mixtures in a pH = 14 electrolyte. Because of its capacity to enable electrode regeneration in the presence of O₂ without affecting H₂ production, an alkaline electrolyte was chosen (Figure 10). This ground-breaking self-healing semiconductor–electrolyte interface provides the electrode with great stability, which is critical for the sustained photoelectrolysis of water [116].

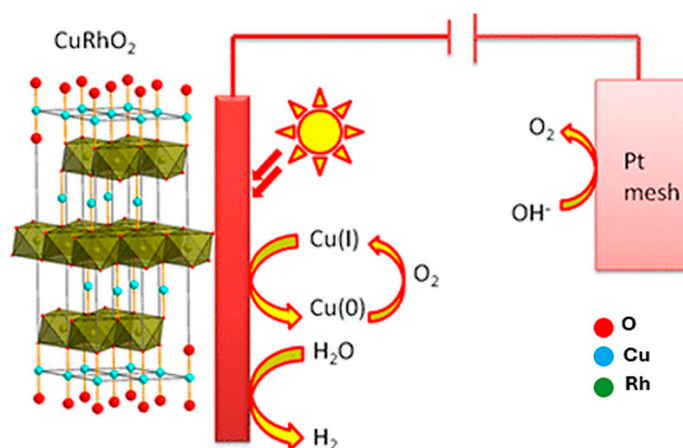


Figure 10. Polycrystalline CuRhO_2 as a photocathode for visible-light-induced water splitting [117].

The photoelectrochemical reduction of water utilizing a CuRhO_2 electrode during visible light irradiation lasted more than 8 h at a potential of -0.9 V versus SCE in 1 M of NaOH exposed to air. The system was stable, as demonstrated by H_2 gas generation detected by the formation of bubbles at the surface of the electrode, which was validated through gas chromatography tests [118]. The electrolyte must be saturated with O_2 (from air or a pure oxygen stream), and the pH must be basic, according to two important conditions for a stable H_2 -producing system. The increased air stability suggests the existence of an interface self-regeneration process.

A CuRhO_2 delafossite photocathode is an ideal choice for water reduction due to its powerful visible-light responsiveness and intrinsic semiconductor of a p-type nature. Polycrystalline electrodes, which are easily produced using solid-state techniques, exhibit water reduction in 1 M of NaOH under exposure to visible light at an underpotential of 0.2 V. Electrode durability is demonstrated by a photocurrent of up to -1.0 mA/cm^2 at -0.9 V in air for at least 8 h. This is the first time an oxygen-driven self-healing process at an electrode–electrolyte interface has been described, highlighting the material’s potential for producing solar fuels from water [119].

7. CuMnO_2 Delafossite Materials

CuMnO_2 has long been explored as a catalyst, particularly in oxygen and hydrogen evolution (OER and HER) processes. CuMnO_2 particles were studied using cyclic voltammetry, electrochemical impedance spectroscopy, and linear sweep voltammetry in a 1 M KOH solution and compared to an Ag/AgCl electrode to demonstrate the possibility of current generation in an alkaline electrolyte with water as an electrolysis process. As proven in this study, the CuMnO_2 electrode for OER and HER exhibits more efficient electrocatalytic activity in a three-electrode arrangement on a potentiostat/galvanostat workstation with electrode rotation than without rotation [120]. The calculation of several electrochemical characteristics for the material, such as total charges, charge accessibility, specific capacitance, electroactive surface area, and electrode surface charge change, offered an in-depth understanding of the material’s catalytic behavior. This study’s findings indicate the potential for HER applications in the cathodic area owing to p-type CuMnO_2 as well as future research into OER stability in the anodic region, as Figure 11 depicts. The findings of this study might contribute to an upsurge in research interest in these earth-abundant complex transition metal oxides for further electrochemical applications [121–123].

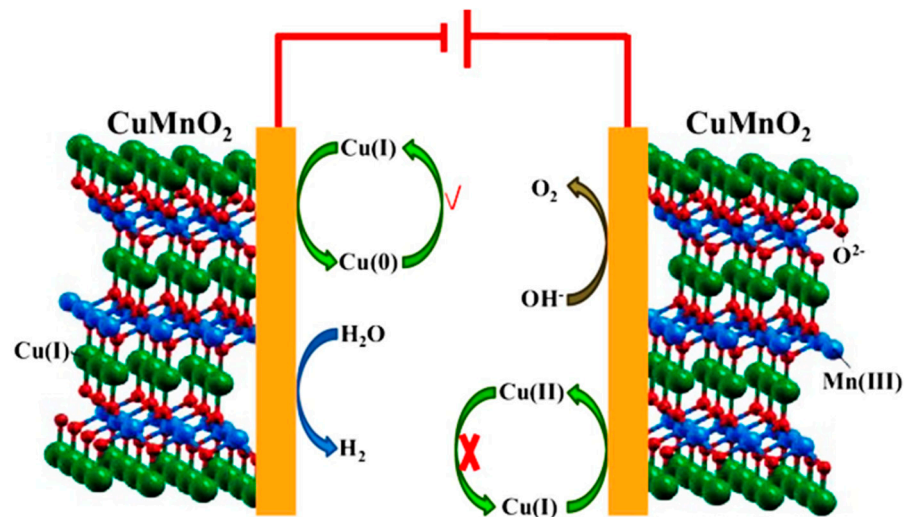


Figure 11. CuMnO₂ bifunctional electrocatalysis: unraveling stability factors in water splitting for OER and HER [121].

8. CuYO₂ Delafossite Materials

The CuYO₂ catalyst has superior electrical conductivity, great stability, and better thermal stability due to its pseudo-delafossite structure. Cu⁺ ions with d-d transitions are found in its layered structure, resulting in a Cu⁺ inter-configuration ranging from 3d⁹4s¹ to 3d¹⁰. The catalyst is made up of tightly coiled multilayered octahedral sites with Y³⁺ ions that share common edges and interact with Cu⁺ ion films in vertical coordination [124]. CuYO₂ additionally features incorporated anionic organisms, which are useful in hydrogen energy research. In our work, we used the self-combustion GNP method to make a CuYO₂ nanopowder catalyst, which we then used in an MSR. CuYO₂ nanopowder precipitated as synthesized in a delafossite structure with a nanosized, spherical shape. During the MSR, the CuYO₂ nanopowder catalyst produced a significant amount of hydrogen while generating very little coke. Table 1 and Figure 12 show temperature profiles for CuCrO₂ and CuFeO₂ nanopowders, CuCrO₂ bulk powder, and an industrial Cu/Al/Zn catalyst.

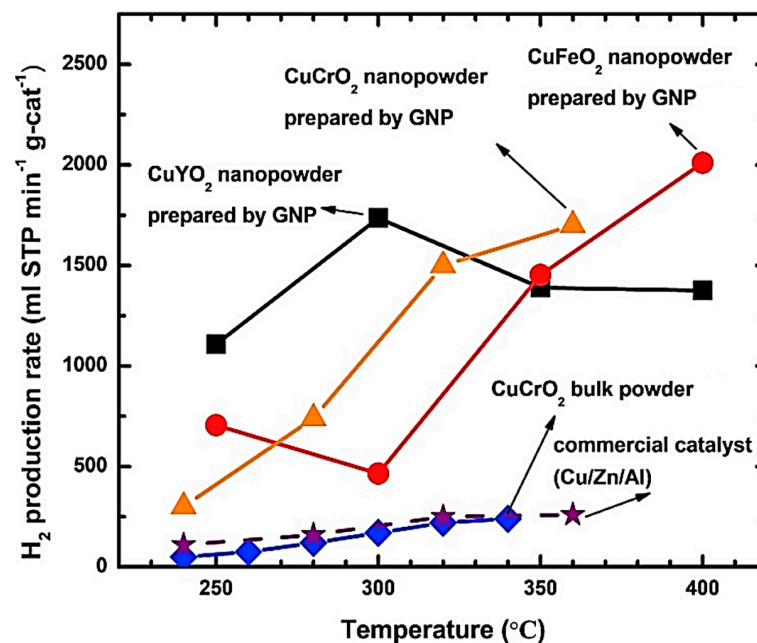


Figure 12. The rates of hydrogen (H₂) generation of CuYO₂ nanopowders after being heated at various temperatures at a flow rate of 30 sccm [125].

Table 1. The rates of hydrogen (H₂) generation of CuYO₂ nanopowders after being heated at various temperatures at a flow rate of 30 sccm.

Catalyst	H ₂ Production Rate (mL STP min ⁻¹ g-cat ⁻¹)				Ref.
	250 °C	300 °C	350 °C	400 °C	
CuYO ₂	1107.9	1735.65	1390.05	1375.2	[95]
CuFeO ₂	705.188	464.869	1452.975	2010.600	[125]
CuCrO ₂	279.169	753.205	1480.365	1720.300	[126]

The MSR catalytic efficiency was investigated in a continuous flow reactor using nitrogen as an intermediate gas. GC-1000 gas separation with a TCD was used to examine the gas products. The H₂ generation rate (mL STP min⁻¹ g-cat⁻¹) was used to assess the efficacy of the CuYO₂ nanopowder catalyst [90,127–131].

A 25 cm quartz pipe with a 1.2 cm internal diameter was used in the testing, and nitrogen was used as a dilutant and gas carrier with a flow rate of 30 sccm. Gas chromatography was used to assess the rate of hydrogen creation, and the catalyst performed better with rotation during the OER and HER. These findings demonstrate the potential of CuYO₂ nanopowder as a viable catalytic material for hydrogen generation applications, including fuel cells, battery devices, electrolyzers, and solar water splitting [102,132–134].

- **Performance table:**

Delafossite Material	Photocatalytic Application	Key Performance Metrics	Notable Features
CuFeO ₂	Solar water reduction	Band-edge location, stability, CO ₂ reduction potential	Sol-gel-based method, excellent band edge location, stability, and CO ₂ reduction capability
CuCrO ₂	Photochemical H ₂ evolution	Band gap, stability visible light responsiveness	Efficient absorption of visible light, stable H ₂ production, potential for co-catalyst integration
CuAlO ₂	Hydrogen Production	Band gap, catalytic aptitude for visible light induced H ₂ generation	Effective H ₂ generation under visible light, dependence on S ²⁻ as a reducing agent
CuRhO ₂	Visible light water splitting	Band edge locations, photostability, self-healing interface	Unique self-healing semiconductor/electrolyte interface, stable H ₂ production under visible light
CuMnO ₂	Oxygen and hydrogen evolution	Electrocatalytic activity, stability	Bifunctional electrocatalysis for OER and HER, potential for further research
CuYO ₂	Methane steam reformation	H ₂ production rate, thermal stability, catalyst efficiency	Superior electrical conductivity, great stability, potential for hydrogen generation applications

- **Active Sites:**

- **CuFeO₂**—Active sites are likely associated with the delafossite structure, with an emphasis on the optimized semiconductor interface using suitable overlayers or catalysts.

- **CuCrO₂**—Active sites include the CuCrO₂ surface where H₂ is primarily liberated, and S₂ is oxidized on the Cu₂O surface when coupled with in situ created n-Cu₂O.
 - **CuAlO₂**—Active sites involve the conduction band's potential, allowing spontaneous H₂ evolution, particularly in the presence of S²⁻ as a reducing agent.
 - **CuRhO₂**—Active sites are attributed to the polycrystalline CuRhO₂ surface, with photogenerated band conduction electrons reducing water and valence band holes oxygenating water.
 - **CuMnO₂**—Active sites for CuMnO₂ are not explicitly mentioned in the provided text, but further research may focus on its electrocatalytic activity for oxygen and hydrogen evolution.
 - **CuYO₂**—Active sites are likely associated with the pseudo-delafossite structure, where Cu⁺ ions with d-d transitions and Y³⁺ ions interact, facilitating hydrogen generation during methane steam reformation.
- **Summary and Comparison:**
- **CuFeO₂**—stands out for its sol-gel-based production method, excellent band-edge location, stability, and potential for CO₂ reduction;
 - **CuCrO₂**—noteworthy for efficient absorption of visible light, stable H₂ production, and potential for co-catalyst integration;
 - **CuAlO₂**—effective in H₂ generation under visible light, particularly with S²⁻ as a reducing agent;
 - **CuRhO₂**—unique for its self-healing semiconductor/electrolyte interface, providing stability for sustained photo electrolysis of water;
 - **CuMnO₂**—limited details provided, emphasizing further research opportunities;
 - **CuYO₂**—superior electrical conductivity, great stability, and potential for hydrogen generation applications during methane steam reforming.

9. Conclusions

In conclusion, hydrogen (H₂) emerges as a pivotal and eco-friendly alternative in the realm of renewable energy, addressing the escalating need for sustainable and clean power. Its significance lies in its potential to alleviate both the energy crisis and climate change, particularly in the industrial sector, where its application in electricity generation results in minimal nitrous and sulfur oxide emissions. However, despite its environmental benefits, challenges persist in the efficient processing and storage of hydrogen, posing obstacles to the full realization of a hydrogen-based energy economy.

One major impediment is the security issues surrounding hydrogen storage, transportation, and utilization, with current conventional storage methods falling short in terms of capacity. To address this limitation, the implementation of a hydrogen storage system based on fuel cells has been proposed, particularly the H₂ fuel cell system, characterized by low carbon emissions and high efficiency. This technology represents a compelling alternative to internal combustion engines, especially in the automotive sector, contributing to the global interest and growth of hydrogen fuel cell systems in recent years.

The exploration of photocatalysts, specifically in the context of water splitting for hydrogen generation, is a key focus. The integration of photoelectrodes into PV-cell-powered configurations showcases the potential of photoelectrochemical (PEC) systems in harnessing solar energy for hydrogen production. However, the choice of semiconductor (SC) material is crucial, necessitating the satisfaction of specific criteria relating to aspects such as band gap and stability to ensure optimal performance.

Delafossite compounds, such as CuMO₂, have garnered attention for their applications in hydrogen generation via PEC water splitting, as well as in optoelectronic devices. Notably, CuFeO₂ has been highlighted as a promising candidate, demonstrating excellent band edge location and stability for efficient water splitting. Its potential extends beyond

hydrogen production, as it also holds promise in reducing CO₂, showcasing the versatility of delafossite materials in addressing multiple environmental challenges.

The conclusions of the studies also delve into the exploration of other delafossite materials, including CuCrO₂, CuAlO₂, CuRhO₂, CuMnO₂, and CuYO₂. Each material exhibits unique properties and catalytic capabilities, contributing to the broader understanding of their potential applications in solar water splitting, oxygen and hydrogen evolution processes, and other areas. Notably, CuRhO₂ stands out because of its self-healing semiconductor/electrolyte interface, representing a breakthrough in achieving stable and sustained photo-electrolysis of water.

Author Contributions: H.C.: Conceptualization, Methodology, Writing—original draft, Experimental works, Summarization, revision. A.B.: Interpretation, Methodology, Validation, Writing—original draft, Revision. B.M.S.: Visualization, Investigation, Supervision, Revision. All authors have read and agreed to the published version of the manuscript.

Funding: This research received no external funding.

Data Availability Statement: All data are included in the manuscript.

Acknowledgments: Amal Bouich acknowledges MCIN for providing funding support through Ministerio de Ciencia e Innovación (Spain) (MCIN/AEI/10.13039/501100011033) and NextGenerationEU.

Conflicts of Interest: The authors declare no conflicts of interest that could have appeared to influence the work reported in this paper. The authors declare that they have no known competing financial or personal interests.

References

1. Younsi, M.; Saadi, S.; Bouguelia, A.; Aider, A.; Trari, M. Synthesis and characterization of oxygen-rich delafossite CuYO_{2+x}—Application to H₂-photo production. *Sol. Energy Mater. Sol. Cells* **2007**, *91*, 1102–1109. [[CrossRef](#)]
2. Sazali, N. Emerging technologies by hydrogen: A review. *Int. J. Hydrogen Energy* **2020**, *45*, 18753–18771. [[CrossRef](#)]
3. Aravindan, M.; Madhan, K.V.; Hariharan, V.S.; Narahari, T.; Arun, K.P.; Madhesh, K.; Praveen, K.J.G.; Prabakaran, R. Fuelling the future: A review of non-renewable hydrogen production and storage techniques. *Renew. Sustain. Energy Rev.* **2023**, *188*, 113791. [[CrossRef](#)]
4. Aravindan, M.; Kumar, P. Hydrogen towards sustainable transition: A review of production, economic, environmental impact and scaling factors. *Results Eng.* **2023**, *20*, 101456.
5. Pahwa, P.K.; Pahwa, G.K. *Hydrogen Economy*; The Energy and Resources Institute (TERI): New Delhi, India, 2014.
6. Sohni, S.; Nidaullah, H.; Gul, K.; Ahmad, I.; Omar, A.M. Nanotechnology for Safe and Sustainable Environment: Realm of Wonders. In *Nanomaterials and Their Fascinating Attributes—Development and Prospective Applications of Nanoscience and Nanotechnology*; Khan, S.B., Asiri, A.M., Akhtar, K., Eds.; Bentham Science Publishers: Sharjah, United Arab Emirates, 2018; Volume 2, pp. 37–117.
7. Sonthalia, A.; Kumar, N.; Tomar, M.; Geo, V.E.; Thiyagarajan, S.; Pugazhendhi, A. Moving ahead from hydrogen to methanol economy: Scope and challenges. *Clean Technol. Environ. Policy* **2021**, *25*, 1–25. [[CrossRef](#)]
8. Mitra, S.; Maiti, D.K. Nanotechnology for green energy and sustainable future. In *Nano Tools and Devices for Enhanced Renewable Energy*; Elsevier: Amsterdam, The Netherlands, 2021; pp. 521–533.
9. Rolo, I.; Costa, V.A.F.; Brito, F.P. Hydrogen-Based Energy Systems: Current Technology Development Status, Opportunities and Challenges. *Energies* **2023**, *17*, 180. [[CrossRef](#)]
10. Koriche, N.; Bouguelia, A.; Aider, A.; Trari, M. Photocatalytic hydrogen evolution over delafossite CuAlO₂. *Int. J. Hydrogen Energy* **2005**, *30*, 693–699. [[CrossRef](#)]
11. Qazi, U.Y. Future of hydrogen as an alternative fuel for next-generation industrial applications; challenges and expected opportunities. *Energies* **2022**, *15*, 4741. [[CrossRef](#)]
12. Ahmed, S.F.; Mofijur, M.; Nuzhat, S.; Rafa, N.; Musharrat, A.; Lam, S.S.; Boretti, A. Sustainable hydrogen production: Technological advancements and economic analysis. *Int. J. Hydrogen Energy* **2022**, *47*, 37227–37255. [[CrossRef](#)]
13. Gholami, F.; Tomas, M.; Gholami, Z.; Vakili, M. Technologies for the nitrogen oxides reduction from flue gas: A review. *Sci. Total Environ.* **2020**, *714*, 136712. [[CrossRef](#)]
14. Larki, I.; Zahedi, A.; Asadi, M.; Forootan, M.M.; Farajollahi, M.; Ahmadi, R.; Ahmadi, A. Mitigation approaches and techniques for combustion power plants flue gas emissions: A comprehensive review. *Sci. Total Environ.* **2023**, *903*, 166108. [[CrossRef](#)] [[PubMed](#)]
15. Panić, I.; Cuculić, A.; Čelić, J. Color-coded hydrogen: Production and storage in maritime sector. *J. Mar. Sci. Eng.* **2022**, *10*, 1995. [[CrossRef](#)]

16. Asghar, U.; Rafiq, S.; Anwar, A.; Iqbal, T.; Ahmed, A.; Jamil, F.; Khurram, M.S.; Akbar, M.M.; Farooq, A.; Shah, N.S.; et al. Review on the progress in emission control technologies for the abatement of CO₂, SO_x and NO_x from fuel combustion. *J. Environ. Chem. Eng.* **2021**, *9*, 106064. [[CrossRef](#)]
17. Farghali, M.; Osman, A.I.; Umetsu, K.; Rooney, D.W. Integration of biogas systems into a carbon zero and hydrogen economy: A review. *Environ. Chem. Lett.* **2022**, *20*, 2853–2927. [[CrossRef](#)]
18. Yu, C.-L.; Sakthinathan, S.; Chen, S.-Y.; Yu, B.-S.; Chiu, T.-W.; Dong, C. Hydrogen generation by methanol steam reforming process by delafossite-type CuYO₂ nanopowder catalyst. *Microporous Mesoporous Mater.* **2021**, *324*, 111305. [[CrossRef](#)]
19. Tzimas, E.; Filiou, C.; Peteves, S.D.; Veyret, J.B. *Hydrogen Storage: State-of-the-Art and Future Perspective*; EUR 20995EN; EU Commission, JRC Petten: Petten, The Netherlands, 2003.
20. Ren, J.; Musyoka, N.M.; Langmi, H.W.; Mathe, M.; Liao, S. Current research trends and perspectives on materials-based hydrogen storage solutions: A critical review. *Int. J. Hydrogen Energy* **2017**, *42*, 289–311. [[CrossRef](#)]
21. Preuster, P.; Alekseev, A.; Wasserscheid, P. Hydrogen storage technologies for future energy systems. *Annu. Rev. Chem. Biomol. Eng.* **2017**, *8*, 445–471. [[CrossRef](#)] [[PubMed](#)]
22. Bérubé, V.; Radtke, G.; Dresselhaus, M.; Chen, G. Size effects on the hydrogen storage properties of nanostructured metal hydrides: A review. *Int. J. Energy Res.* **2007**, *31*, 637–663. [[CrossRef](#)]
23. Gary, S. State-of-the-art review of hydrogen storage in reversible metal hydrides for military fuel cell applications. *Final. Rep. Contract* **1997**, *14*, 1–159.
24. Yang, J.; Sudik, A.; Wolverton, C.; Siegel, D.J. High capacity hydrogen storage materials: Attributes for automotive applications and techniques for materials discovery. *Chem. Soc. Rev.* **2010**, *39*, 656–675. [[CrossRef](#)]
25. Liu, Q.-L.; Zhao, Z.-Y.; Zhao, R.-D.; Yi, J.-H. Fundamental properties of delafossite CuFeO₂ as photocatalyst for solar energy conversion. *J. Alloys Compd.* **2020**, *819*, 153032. [[CrossRef](#)]
26. Sorensen, B. *Hydrogen and Fuel Cells: Emerging Technologies and Applications*; Academic Press: Cambridge, MA, USA, 2011.
27. Cavaliere, P. Hydrogen and Energy Transition. In *Water Electrolysis for Hydrogen Production*; Springer International Publishing: Cham, Switzerland, 2023; pp. 61–104.
28. National Research Council. *The Hydrogen Economy: Opportunities, Costs, Barriers, and R&D Needs*; National Academies Press: Washington, DC, USA, 2004.
29. Greene, D.L. Transportation and energy. In *The Geography of Urban Transportation*; The Guilford Press: New York, NY, USA, 2004; pp. 274–294.
30. Kroyan, Y.; Wojcieszak, M. *End-Use Performance of Alternative Fuels in Various Modes of Transportation*; ADVANCEFUEL project Deliverable D; Aalto University: Espoo, Finland, 2020; Volume 5, p. 5.
31. Das, P.K.; Jiao, K.; Wang, Y.; Barbir, F.; Li, X. (Eds.) *Fuel Cells for Transportation: Fundamental Principles and Applications*; Woodhead Publishing: Sawston, UK, 2023.
32. Benghanem, M.; Mellit, A.; Almohamadi, H.; Haddad, S.; Chettibi, N.; Alanazi, A.M.; Dasalla, D.; Alzahrani, A. Hydrogen production methods based on solar and wind energy: A review. *Energies* **2023**, *16*, 757. [[CrossRef](#)]
33. Paumo, H.K.; Dalhatou, S.; Katata-Seru, L.M.; Kamdem, B.P.; Tijani, J.O.; Vishwanathan, V.; Kane, A.; Bahadur, I. TiO₂ assisted photocatalysts for degradation of emerging organic pollutants in water and wastewater. *J. Mol. Liq.* **2021**, *331*, 115458. [[CrossRef](#)]
34. Li, T. Synthesis, Characterisation and Photocatalytic Activity of Porous Silicon-Based Materials. Doctoral Dissertation, University of East Anglia, Norwich, UK, 2017.
35. Serrà, A.; Philippe, L.; Perreault, F.; Garcia-Segura, S. Photocatalytic treatment of natural waters. Reality or hype? The case of cyanotoxins remediation. *Water Res.* **2020**, *188*, 116543. [[CrossRef](#)]
36. Guan, D.; Wang, B.; Zhang, J.; Shi, R.; Jiao, K.; Li, L.; Wang, Y.; Xie, B.; Zhang, Q.; Yu, J.; et al. Hydrogen society: From present to future. *Energy Environ. Sci.* **2023**, *16*, 4926–4943. [[CrossRef](#)]
37. Bellal, B.; Saadi, S.; Koriche, N.; Bouguelia, A.; Trari, M. Physical properties of the delafossite LaCuO₂. *J. Phys. Chem. Solids* **2009**, *70*, 1132–1136. [[CrossRef](#)]
38. He, H. *Solution Processed Metal Oxide Thin Films for Electronic Applications*; School of Materials Science and Engineering, Zhejiang University: Hangzhou, China, 2020; p. 7.
39. Lee, L.C. Vapour-Based Growth of Inorganic Compounds for Next-Generation, Stable Photovoltaics. Doctoral Dissertation, University of Cambridge, Cambridge, UK, 2020.
40. Wildsmith, T. Low Temperature Precursors for SnO_x Thin Films. Doctoral Dissertation, University of Bath, Bath, UK, 2014.
41. Sheets, W.C. Synthetic Methods for Multifunctional Materials. Doctoral Dissertation, Northwestern University, Evanston, IL, USA, 2006.
42. Karatas, Y.; Zengin, A.; Gülcan, M. Preparation and characterization of amine-terminated delafossite type oxide, CuMnO₂-NH₂, supported Pd (0) nanoparticles for the H₂ generation from the methanolysis of ammonia-borane. *Int. J. Hydrogen Energy* **2022**, *47*, 16036–16046. [[CrossRef](#)]
43. Sivagurunathan, A.T.; Adhikari, S.; Kim, D.-H. Strategies and implications of atomic layer deposition in photoelectrochemical water splitting: Recent advances and prospects. *Nano Energy* **2021**, *83*, 105802. [[CrossRef](#)]
44. Chatterjee, P.; Ambati, M.S.K.; Chakraborty, A.K.; Chakraborty, S.; Biring, S.; Ramakrishna, S.; Wong, T.K.S.; Kumar, A.; Lawaniya, R.; Dalapati, G.K. Photovoltaic/photo-electrocatalysis integration for green hydrogen: A review. *Energy Convers. Manag.* **2022**, *261*, 115648. [[CrossRef](#)]

45. Prévot, M.S.; Sivula, K. Photoelectrochemical tandem cells for solar water splitting. *J. Phys. Chem. C* **2013**, *117*, 17879–17893. [CrossRef]
46. Desai, M.A.; Vyas, A.N.; Saratale, G.D.; Sartale, S.D. Zinc oxide superstructures: Recent synthesis approaches and application for hydrogen production via photoelectrochemical water splitting. *Int. J. Hydrogen Energy* **2019**, *44*, 2091–2127. [CrossRef]
47. Kalanur, S.S.; Duy, L.T.; Seo, H. Recent Progress in Photoelectrochemical Water Splitting Activity of WO₃ Photoanodes. *Top. Catal.* **2018**, *61*, 1043–1076. [CrossRef]
48. Wang, K.; Huang, D.; Li, X.; Feng, K.; Shao, M.; Yi, J.; He, W.; Qiao, L. Unconventional strategies to break through the efficiency of light-driven water splitting: A review. *Electron* **2023**, *1*, e4. [CrossRef]
49. Gurunathan, K.; Baeg, J.-O.; Lee, S.M.; Subramanian, E.; Moon, S.-J.; Kong, K.-J. Visible light assisted highly efficient hydrogen production from H₂S decomposition by CuGaO₂ and CuGa_{1-x}In_xO₂ delafossite oxides bearing nanostructured co-catalysts. *Catal. Commun.* **2008**, *9*, 395–402. [CrossRef]
50. Ke, J. Artificial photosynthesis and solar fuels. In *Solar-to-Chemical Conversion: Photocatalytic and Photoelectrochemical Processes*; Wiley: Hoboken, NJ, USA, 2021; pp. 7–39.
51. Shi, Q.; Duan, H. Recent progress in photoelectrocatalysis beyond water oxidation. *Chem Catal.* **2022**, *2*, 3471–3496. [CrossRef]
52. Qi, S.; Guo, R.; Bi, Z.; Zhang, Z.; Li, C.; Pan, W. Recent Progress of Covalent Organic Frameworks-Based Materials in Photocatalytic Applications: A Review. *Small* **2023**, *19*, e2303632. [CrossRef]
53. Aboagye, D.; Djellabi, R.; Medina, F.; Contreras, S. Radical-mediated photocatalysis for lignocellulosic biomass conversion into value-added chemicals and hydrogen: Facts, opportunities and challenges. *Angew. Chem. Int. Ed.* **2023**, *62*, e202301909. [CrossRef]
54. Curti, M.; AlSalka, Y.; Al-Madanat, O.; Bahnemann, D.W. Isotopic Substitution to Unravel the Mechanisms of Photocatalytic Hydrogen Production. In *Photocatalytic Hydrogen Production for Sustainable Energy*; Wiley: Hoboken, NJ, USA, 2023; pp. 35–61.
55. Bagtache, R.; Brahimi, R.; Mahroua, O.; Boudjellal, L.; Abdmeziem, K.; Trari, M. Photoelectrochemical study of the delafossite agnio₂ nanostructure: Application to hydrogen production. *J. Electrochem. Energy Convers. Storage* **2020**, *17*, 031008. [CrossRef]
56. Qiu, W.-T.; Huang, Y.-C.; Wang, Z.-L.; Xiao, S.; Ji, H.-B.; Tong, Y.-X. Effective strategies towards high-performance photoanodes for photoelectrochemical water splitting. *Acta Phys. Chim. Sin.* **2017**, *33*, 80–102. [CrossRef]
57. Bagnall, A.J. Novel Electrode and Photoelectrode Materials for Hydrogen Production Based on Molecular Catalysts. Doctoral Dissertation, Université Grenoble Alpes, Saint-Martin-d'Hères, France, Uppsala Universitet, Uppsala, Sweden, 2022.
58. Minero, C.; Maurino, V. 16 Solar Photocatalysis for Hydrogen Production and CO₂ Conversion. In *Catalysis for Renewables: From Feedstock to Energy Production*; Wiley: Hoboken, NJ, USA, 2007; p. 351.
59. Knöppel, J. On the Stability of Anode (Photo-) Electrocatalysts in the Solar to Hydrogen Nexus. Doctoral Dissertation, Friedrich-Alexander-Universität Erlangen-Nürnberg (FAU), Erlangen, Germany, 2022.
60. Liu, Q.L.; Zhao, Z.Y.; Yi, J.H. Excess oxygen in delafossite CuFeO_{2+δ}: Synthesis, characterization, and applications in solar energy conversion. *Chem. Eng. J.* **2020**, *396*, 125290. [CrossRef]
61. Mazloomi, K.; Sulaiman, N.B.; Moayedi, H. Electrical efficiency of electrolytic hydrogen production. *Int. J. Electrochem. Sci.* **2012**, *7*, 3314–3326. [CrossRef]
62. Sato, M.; Mooney, H.M. The electrochemical mechanism of sulfide self-potentials. *Geophysics* **1960**, *25*, 226–249. [CrossRef]
63. Peled, E.; Golodnitsky, D.; Ardel, G. Advanced model for solid electrolyte interphase electrodes in liquid and polymer electrolytes. *J. Electrochem. Soc.* **1997**, *144*, L208–L210. [CrossRef]
64. Zaban, A.; Zinigrad, E.; Aurbach, D. Impedance spectroscopy of Li electrodes. 4. A general simple model of the Li– solution interphase in polar aprotic systems. *J. Phys. Chem.* **1996**, *100*, 3089–3101. [CrossRef]
65. Huda, M.N.; Yan, Y.; Walsh, A.; Wei, S.-H.; Turner, J.A.; Al-Jassim, M.M. Delafossite-alloy photoelectrodes for PEC hydrogen production: A density functional theory study. In Proceedings of the SPIE—The International Society for Optical Engineering 7770, Solar Hydrogen and Nanotechnology V, San Diego, CA, USA, 24 August 2010; Volume 7770, pp. 45–54.
66. Götzendörfer, S. Synthesis of Copper-Based Transparent Conductive Oxides with Delafossite Structure Via Sol-Gel Processing. Doctoral Dissertation, Universität Würzburg, Würzburg, Germany, 2010.
67. Liu, Y. P-Type Transparent Conducting Oxides Synthesized by Electrohydrodynamic Process. Doctoral Dissertation, Alfred University, Alfred, NY, USA, 2017.
68. Manoj, R.; Jayaraj, M.K. Characterisation of Transparent Conducting Thin Films Grown by Pulsed Laser Deposition and RF Magnetron Sputtering. Ph.D. Thesis, Department of Physics, Kerala, India, 2006.
69. Bishop, P.T.; Sutton, P.A.; Gardener, M.; Wakefield, G. Novel Transparent Conducting Oxide Technology for Solar Cells. 2005. Available online: <https://www.osti.gov/etdeweb/biblio/20714899> (accessed on 23 January 2024).
70. Prévot, M.S.; Guijarro, N.; Sivula, K. Enhancing the performance of a robust sol-gel-processed p-type delafossite CuFeO₂ photocathode for solar water reduction. *ChemSusChem* **2015**, *8*, 1359–1367. [CrossRef] [PubMed]
71. Wang, S.C.; Tang, F.Q.; Wang, L.Z. Visible light responsive metal oxide photoanodes for photoelectrochemical water splitting: A comprehensive review on rational materials design. *J. Inorg. Mater.* **2018**, *33*, 173–196.
72. Gan, J.; Lu, X.; Tong, Y. Towards highly efficient photoanodes: Boosting sunlight-driven semiconductor nanomaterials for water oxidation. *Nanoscale* **2014**, *6*, 7142–7164. [CrossRef]
73. Liu, J.; Luo, Z.; Mao, X.; Dong, Y.; Peng, L.; Sun-Waterhouse, D.; Kennedy, J.V.; Waterhouse, G.I.N. Recent Advances in Self-Supported Semiconductor Heterojunction Nanoarrays as Efficient Photoanodes for Photoelectrochemical Water Splitting. *Small* **2022**, *18*, e2204553. [CrossRef]

74. Luan, P. *Regulating Bulk and Surface Charge Behaviour of Photoanodes for Enhanced Solar Water Oxidation Efficiency*; Monash University: Mulgrave, Australia, 2019.
75. Prasad, U. BiVO₄-Based Photoanodes for Photoelectrochemical Water Splitting. In *Clean Energy Materials*; American Chemical Society: Washington, DC, USA, 2020; pp. 137–167.
76. Zhao, Q.M.; Zhao, Z.Y.; Liu, Q.L.; Yao, G.Y.; Dong, X.D. Delafossite CuGaO₂ as promising visible-light-driven photocatalyst: Synthesize, properties, and performances. *J. Phys. D Appl. Phys.* **2020**, *53*, 135102. [[CrossRef](#)]
77. Pawar, R.C.; Lee, C.S. *Heterogeneous Nanocomposite-Photocatalysis for Water Purification*; William Andrew: Norwich, NY, USA, 2015; ISBN 9780323393102.
78. Calbo, J. Dye-Sensitized Solar Cells: Past, Present and Future. In *Photoenergy and Thin Film Materials*; Wiley: Hoboken, NJ, USA, 2019; pp. 49–119.
79. Prévot, M.S. *Investigating and Controlling Charge Carrier Behavior in p-Type Delafossite CuFeO₂ Photocathodes for Solar Fuel Production*; EPFL: Lausanne, Switzerland, 2017.
80. Li, Z.; Luo, W.; Zhang, M.; Feng, J.; Zou, Z. Photoelectrochemical cells for solar hydrogen production: Current state of promising photoelectrodes, methods to improve their properties, and outlook. *Energy Environ. Sci.* **2013**, *6*, 347–370. [[CrossRef](#)]
81. Fabre, B.; Loget, G. Silicon Photoelectrodes Prepared by Low-Cost Wet Methods for Solar Photoelectrocatalysis. *Accounts Mater. Res.* **2023**, *4*, 133–142. [[CrossRef](#)]
82. Moss, B.; Babacan, O.; Kafizas, A.; Hankin, A. A review of inorganic photoelectrode developments and reactor scale-up challenges for solar hydrogen production. *Adv. Energy Mater.* **2021**, *11*, 2003286. [[CrossRef](#)]
83. Woodhouse, M.; Parkinson, B.A. Combinatorial approaches for the identification and optimization of oxide semiconductors for efficient solar photoelectrolysis. *Chem. Soc. Rev.* **2009**, *38*, 197–210. [[CrossRef](#)] [[PubMed](#)]
84. Esposito, D.V.; Baxter, J.B.; John, J.; Lewis, N.S.; Moffat, T.P.; Ogitsu, T.; O’Neil, G.D.; Pham, T.A.; Talin, A.A.; Velazquez, J.M.; et al. Methods of photoelectrode characterization with high spatial and temporal resolution. *Energy Environ. Sci.* **2015**, *8*, 2863–2885. [[CrossRef](#)]
85. Ahmed, J.; Mao, Y. Delafossite CuAlO₂ nanoparticles with electrocatalytic activity toward oxygen and hydrogen evolution reactions. In *Nanomaterials for Sustainable Energy*; American Chemical Society: Washington, DC, USA, 2015; pp. 57–72.
86. Li, C.; He, J.; Xiao, Y.; Li, Y.; Delaunay, J.-J. Earth-abundant Cu-based metal oxide photocathodes for photoelectrochemical water splitting. *Energy Environ. Sci.* **2020**, *13*, 3269–3306. [[CrossRef](#)]
87. Díez-García, M.I.; Gómez, R. Progress in ternary metal oxides as photocathodes for water splitting cells: Optimization strategies. *Sol. RRL* **2022**, *6*, 2100871. [[CrossRef](#)]
88. Monllor-Satoca, D.; Díez-García, M.I.; Lana-Villarreal, T.; Gómez, R. Photoelectrocatalytic production of solar fuels with semiconductor oxides: Materials, activity and modeling. *Chem. Commun.* **2020**, *56*, 12272–12289. [[CrossRef](#)] [[PubMed](#)]
89. Axel, F. Synthesis and Characterisation of Delafossite CuFeO₂ for Solar Energy Applications. 2016. Available online: <http://urn.kb.se/resolve?urn=urn:nbn:se:uu:diva-297710> (accessed on 23 January 2024).
90. Sullivan, I.; Zoellner, B.; Maggard, P.A. Copper(I)-based p-type oxides for photoelectrochemical and photovoltaic solar energy conversion. *Chem. Mater.* **2016**, *28*, 5999–6016. [[CrossRef](#)]
91. Maggard, P.A. Discovery and Development of Semiconductors and Structures for Photoelectrochemical Energy Conversion. In *Springer Handbook of Inorganic Photochemistry*; Springer International Publishing: Cham, Switzerland, 2022; pp. 805–850.
92. Shan, B.-F.; Chen, X.-L.; Zhao, Z.-Y. Band engineering of delafossite CuB_{1-x}Fe_xO₂ (B = Al, Cr, Sc) solid solutions as photocathodes: Visible-light response and performance enhancement. *Int. J. Hydrogen Energy* **2023**, *51*, 499–510. [[CrossRef](#)]
93. Beatricevena, T.; Murthy, A.S.R.; Prabhu, E.; Gnanasekar, K. Wide range hydrogen sensing behavior of a silver delafossite: Performance towards long term stability, repeatability and selectivity. *Int. J. Hydrogen Energy* **2021**, *46*, 2824–2834. [[CrossRef](#)]
94. Tang, B.; Xiao, F.-X. An overview of solar-driven photoelectrochemical CO₂ conversion to chemical fuels. *ACS Catal.* **2022**, *12*, 9023–9057. [[CrossRef](#)]
95. Hsu, K.-C.; Keyan, A.K.; Hung, C.-W.; Sakthinathan, S.; Yu, C.-L.; Chiu, T.-W.; Nagaraj, K.; Fan, F.-Y.; Shan, Y.-K.; Chen, P.-C. Fabrication of CuYO₂ Nanofibers by Electrospinning and Applied to Hydrogen Harvest. *Materials* **2022**, *15*, 8957. [[CrossRef](#)]
96. Son, H.; Uthirakumar, P.; Park, J.H.; Park, J.-H.; Woo, S.; Kim, C.Y. Investigation of non-stoichiometric delafossite photoelectrodes composed of cuprous oxide and iron oxide for enhanced water-splitting. *J. Alloy. Compd.* **2023**, *948*, 169781. [[CrossRef](#)]
97. Derbal, A.; Omeiri, S.; Bouguelia, A.; Trari, M. Characterization of new heterosystem CuFeO₂/SnO₂ application to visible-light induced hydrogen evolution. *Int. J. Hydrogen Energy* **2008**, *33*, 4274–4282. [[CrossRef](#)]
98. Li, G.; Khim, S.; Chang, C.S.; Fu, C.; Nandi, N.; Li, F.; Yang, Q.; Blake, G.R.; Parkin, S.; Auffermann, G.; et al. In situ modification of a delafossite-type PdCoO₂ bulk single crystal for reversible hydrogen sorption and fast hydrogen evolution. *ACS Energy Lett.* **2019**, *4*, 2185–2191. [[CrossRef](#)] [[PubMed](#)]
99. Bouich, A.; Torres, J.C.; Chfii, H.; Mari-Guaita, J.; Khattak, Y.H.; Baig, F.; Soucase, B.M.; Palacios, P. Delafossite as hole transport layer a new pathway for efficient perovskite-based solar cells: Insight from experimental, DFT and numerical analysis. *Sol. Energy* **2023**, *250*, 18–32. [[CrossRef](#)]
100. Chfii, H.; Bouich, A.; Soucase, B.M.; Abdlefdil, M. A new approach for growing high-quality delafossite CuCoO₂ films by spray pyrolysis through the optimization of the Cu/Co ratio. *Opt. Mater.* **2023**, *135*, 113229. [[CrossRef](#)]

101. Chfii, H.; Bouich, A.; Andrio, A.; Torres, J.C.; Soucase, B.M.; Palacios, P.; Abd Lefdil, M.; Compañ, V. The Structural and Electrochemical Properties of CuCoO₂ Crystalline Nanopowders and Thin Films: Conductivity Experimental Analysis and Insights from Density Functional Theory Calculations. *Nanomaterials* **2023**, *13*, 2312. [[CrossRef](#)] [[PubMed](#)]
102. Chfii, H.; Bouich, A.; Soucase, B.M.; Abd-Lefdil, M. Structural and physical properties of Mg-doped CuCoO₂ delafossite thin films. *Mater. Chem. Phys.* **2023**, *306*, 128006. [[CrossRef](#)]
103. Yengantiwar, A.; Shinde, P.S.; Pan, S.; Gupta, A. Delafossite CuFeO₂ photocathodes grown by direct liquid injection chemical vapor deposition for efficient photoelectrochemical water reduction. *J. Electrochem. Soc.* **2018**, *165*, H831–H837. [[CrossRef](#)]
104. Díaz-García, A.K.; Lana-Villarreal, T.; Gómez, R. Sol–gel copper chromium delafossite thin films as stable oxide photocathodes for water splitting. *J. Mater. Chem. A* **2015**, *3*, 19683–19687. [[CrossRef](#)]
105. Brahimi, R.; Bessekhouad, Y.; Bouguelia, A.; Trari, M. CuAlO₂/TiO₂ heterojunction applied to visible light H₂ production. *J. Photochem. Photobiol. A Chem.* **2007**, *186*, 242–247. [[CrossRef](#)]
106. Beatriceveena, T.V.; Agarwal, L. Highly Selective Behavior of a Silver Delafossite: Response Towards Wide Range of Hydrogen, Repeatability and Long Term Performance. In Proceedings of the 239th ECS Meeting, Chicago, IL, USA, 30 May–3 June 2021; The Electrochemical Society, Inc.: Pennington, NJ, USA, 2021; p. 1443. [[CrossRef](#)]
107. Ma, Y.; Zhou, X.; Ma, Q.; Litke, A.; Liu, P.; Zhang, Y.; Li, C.; Hensen, E.J.M. Photoelectrochemical Properties of CuCrO₂: Characterization of Light Absorption and Photocatalytic H₂ Production Performance. *Catal. Lett.* **2014**, *144*, 1487–1493. [[CrossRef](#)]
108. Crespo, C.T. Potentiality of CuFeO₂-delafossite as a solar energy converter. *Sol. Energy* **2018**, *163*, 162–166. [[CrossRef](#)]
109. Benreguia, N.; Abdi, A.; Mahroua, O.; Trari, M. Photoelectrochemical properties of the crednerite CuMnO₂ and its application to hydrogen production and Mⁿ⁺ reduction (Mn⁺ = Cd²⁺, Pd²⁺, Zn²⁺, Ni²⁺, and Ag⁺). *J. Mater. Sci. Mater. Electron.* **2021**, *32*, 10498–10509. [[CrossRef](#)]
110. Mao, L.; Mohan, S.; Gupta, S.K.; Mao, Y. Multifunctional delafossite CuFeO₂ as water splitting catalyst and rhodamine B sensor. *Mater. Chem. Phys.* **2022**, *278*, 125643. [[CrossRef](#)]
111. Hadia, N.M.A.; Shaban, M.; Ahmed, A.M.; Mohamed, W.S.; Alzaid, M.; Ezzeldien, M.; Hasaneen, M.F.; Malti, W.E.; Abdelazeez, A.A.A.; Rabia, M. Photoelectrochemical Conversion of Sewage Water into H₂ Fuel over the CuFeO₂/CuO/Cu Composite Electrode. *Catalysts* **2023**, *13*, 456. [[CrossRef](#)]
112. Toyoda, K.; Hinogami, R.; Miyata, N.; Aizawa, M. Calculated descriptors of catalytic activity for water electrolysis anode: Application to delafossite oxides. *J. Phys. Chem. C* **2015**, *119*, 6495–6501. [[CrossRef](#)]
113. Trari, M.; Bouguelia, A.; Bessekhouad, Y. p-Type CuYO₂ as hydrogen photocathode. *Sol. Energy Mater. Sol. Cells* **2006**, *90*, 190–202. [[CrossRef](#)]
114. Read, C.G.; Park, Y.; Choi, K.-S. Electrochemical synthesis of p-type CuFeO₂ electrodes for use in a photoelectrochemical cell. *J. Phys. Chem. Lett.* **2012**, *3*, 1872–1876. [[CrossRef](#)] [[PubMed](#)]
115. Lee, T.; Ferri, M.; Piccinin, S.; Selloni, A. Structure, Electronic Properties, and Defect Chemistry of Delafossite CuRhO₂ Bulk and Surfaces. *Chem. Mater.* **2022**, *34*, 1567–1577. [[CrossRef](#)]
116. Huda, M.N.; Yan, Y.; Deutsch, T.; Al-Jassim, M.M.; Turner, A.J.A. *II. F. 7 Photoelectrochemical Materials: Theory and Modeling*; University of Texas at Arlington: Arlington, TX, USA, 2012.
117. Gu, J.; Yan, Y.; Krizan, J.W.; Gibson, Q.D.; Detweiler, Z.M.; Cava, R.J.; Bocarsly, A.B. p-Type CuRhO₂ as a Self-Healing Photoelectrode for Water Reduction under Visible Light. *J. Am. Chem. Soc.* **2014**, *136*, 830–833. [[CrossRef](#)] [[PubMed](#)]
118. Varga, A.; Samu, G.F.; Janáky, C. Rapid synthesis of interconnected CuCrO₂ nanostructures: A promising electrode material for photoelectrochemical fuel generation. *Electrochimica Acta* **2018**, *272*, 22–32. [[CrossRef](#)]
119. Ali, A.H.; Ahmed, A.M.; Abdelhamied, M.M.; Abdel-Khaliek, A.A.; Abd El Khalik, S.; Abass, S.M.; Shaban, M.; Hasan, F.; Rabia, M. Synthesis of lead-free Cu/CuFeO₂/CZTS thin film as a novel photocatalytic hydrogen generator from wastewater and solar cell applications. *Res. Sq.* **2023**. [[CrossRef](#)]
120. Liu, J.; Hu, Q.; Wang, Y.; Yang, Z.; Fan, X.; Liu, L.-M.; Guo, L. Achieving delafossite analog by in situ electrochemical self-reconstruction as an oxygen-evolving catalyst. *Proc. Natl. Acad. Sci. USA* **2020**, *117*, 21906–21913. [[CrossRef](#)]
121. Gu, J.; Wuttig, A.; Krizan, J.W.; Hu, Y.; Detweiler, Z.M.; Cava, R.J.; Bocarsly, A.B. Mg-doped CuFeO₂ photocathodes for photoelectrochemical reduction of carbon dioxide. *J. Phys. Chem. C* **2013**, *117*, 12415–12422. [[CrossRef](#)]
122. Choi, S.Y.; Kim, C.-D.; Han, D.S.; Park, H. Facilitating hole transfer on electrochemically synthesized p-type CuAlO₂ films for efficient solar hydrogen production from water. *J. Mater. Chem. A* **2017**, *5*, 10165–10172. [[CrossRef](#)]
123. Prévot, M.S.; Jeanbourquin, X.A.; Bourée, W.S.; Abdi, F.; Friedrich, D.; van de Krol, R.; Guijarro, N.; Le Formal, F.; Sivula, K. Evaluating charge carrier transport and surface states in CuFeO₂ photocathodes. *Chem. Mater.* **2017**, *29*, 4952–4962. [[CrossRef](#)]
124. Schmachtenberg, N.; Silvestri, S.; Salla, J.d.S.; Dotto, G.L.; Hotza, D.; Jahn, S.L.; Foletto, E.L. Preparation of delafossite-type CuFeO₂ powders by conventional and microwave-assisted hydrothermal routes for use as photo-Fenton catalysts. *J. Environ. Chem. Eng.* **2019**, *7*, 102954. [[CrossRef](#)]
125. Yu, C.-L.; Sakthinathan, S.; Hwang, B.-Y.; Lin, S.-Y.; Chiu, T.-W.; Yu, B.-S.; Fan, Y.-J.; Chuang, C. CuFeO₂-CeO₂ nanopowder catalyst prepared by self-combustion glycine nitrate process and applied for hydrogen production from methanol steam reforming. *Int. J. Hydrogen Energy* **2020**, *45*, 15752–15762. [[CrossRef](#)]
126. Chiu, T.-W.; Hong, R.-T.; Yu, B.-S.; Huang, Y.-H.; Kameoka, S.; Tsai, A.-P. Improving steam-reforming performance by nanopowdering CuCrO₂. *Int. J. Hydrogen Energy* **2014**, *39*, 14222–14226. [[CrossRef](#)]

127. Guan, D.; Xu, H.; Zhang, Q.; Huang, Y.; Shi, C.; Chang, Y.; Xu, X.; Tang, J.; Gu, Y.; Pao, C.; et al. Identifying a universal activity descriptor and a unifying mechanism concept on perovskite oxides for green hydrogen production. *Adv. Mater.* **2023**, *35*, e2305074. [[CrossRef](#)] [[PubMed](#)]
128. Walsh, A.; Ahn, K.-S.; Shet, S.; Huda, M.N.; Deutsch, T.G.; Wang, H.; Turner, J.A.; Wei, S.-H.; Yan, Y.; Al-Jassim, M.M. Ternary cobalt spinel oxides for solar driven hydrogen production: Theory and experiment. *Energy Environ. Sci.* **2009**, *2*, 774–782. [[CrossRef](#)]
129. Zhao, Z.-Y.; Liu, Q.-L. Rational Design of a Two-Dimensional Janus $\text{CuFeO}_{2+\delta}$ Single Layer as a Photocatalyst and Photoelectrode. *J. Phys. Chem. Lett.* **2021**, *12*, 10863–10873. [[CrossRef](#)] [[PubMed](#)]
130. Keyan Arjunan, K.; Rajakumaran, R.; Sakthinathan, S.; Chen, S.M.; Chiu, T.W.; Vinothini, S. Efficient electrocatalyst for hydrogen evolution reaction based on N-rGO-MWCNT/CuAlO₂ nanocomposite in acidic media. *ECS J. Solid State Sci. Technol.* **2021**, *10*, 045011. [[CrossRef](#)]
131. Bouich, A.; Pradas, I.G.; Khan, M.A.; Khattak, Y.H. Opportunities, Challenges, and Future Prospects of the Solar Cell Market. *Sustainability* **2023**, *15*, 15445. [[CrossRef](#)]
132. Bouich, A.; Torres, J.C.; Khattak, Y.H.; Baig, F.; Mari-Guaita, J.; Soucase, B.M.; Mendez-Blas, A.; Palacios, P. Bright future by controlling α/δ phase junction of formamidinium lead iodide doped by imidazolium for solar cells: Insight from experimental, DFT calculations and SCAPS simulation. *Surf. Interfaces* **2023**, *40*, 103159. [[CrossRef](#)]
133. Bouich, A.; Mari-Guaita, J.; Soucase, B.M.; Palacios, P. Bright future by enhancing the stability of methylammonium lead triiodide perovskites thin films through Rb, Cs and Li as dopants. *Mater. Res. Bull.* **2023**, *163*, 112213. [[CrossRef](#)]
134. Bouich, A.; Mari-Guaita, J.; Baig, F.; Khattak, Y.H.; Soucase, B.M.; Palacios, P. Investigation of the surface coating, humidity degradation, and recovery of perovskite film phase for solar-cell applications. *Nanomaterials* **2022**, *12*, 3027. [[CrossRef](#)]

Disclaimer/Publisher's Note: The statements, opinions and data contained in all publications are solely those of the individual author(s) and contributor(s) and not of MDPI and/or the editor(s). MDPI and/or the editor(s) disclaim responsibility for any injury to people or property resulting from any ideas, methods, instructions or products referred to in the content.